2008-02-01

Development of a Three Dimensional Prolapse Model to Simulate Physiological Haemodynamics in a Stented Coronary Artery

Jonathan Murphy
Technological University Dublin, jonathan.murphy@tudublin.ie

Fergal Boyle
Technological University Dublin, fergal.boyle@tudublin.ie

Funder: Department of Mechanical Engineering, Technological University Dublin (DIT)and the Irish Research Council for Science Engineering and Technology (IRCSET)

DEVELOPMENT OF A THREE DIMENSIONAL PROLAPSE MODEL TO SIMULATE PHYSIOLOGICAL HAEMODYNAMICS IN A STENTED CORONARY ARTERY

Jonathan Murphy, Fergal Boyle
Department of Mechanical Engineering
Dublin Institute of Technology
Bolton Street, Dublin 1
Ireland
jonathan.murphy@dit.ie

ABSTRACT
Coronary stent implantation can improve blood flow in an artery that has been narrowed by the build up of arterial plaque. However, the haemodynamic effect of stent placement is unclear and may influence arterial restenosis (re-blockage). The degree of tissue prolapse between stent struts may be an important factor in predicting the restenosis rate of a stent due to the haemodynamic influence of the protruding tissue. In this paper a mathematical model has been developed to numerically predict the tissue prolapse for an artery implanted with a coronary stent. The prolapse model has been applied to the Gianturco-Roubin II (GR-II) coil stent (Cook, USA) and the Palmaz-Schatz (PS) slotted tube stent (Johnson & Johnson, USA). Finally, computational fluid dynamics (CFD) is used to predict the blood flow through both stented arteries with the tissue protrusion as predicted by the prolapse model.

KEY WORDS
Computational fluid dynamics, coronary stent, and tissue prolapse

1. Introduction

The accumulation of fatty cells in the wall of an artery is commonly referred to as an atheromatous plaque or stenosis. A stenosis can significantly reduce the blood flow through the artery. The development of one of more stenoses in the arteries which supply blood to the heart muscle is a condition known as coronary artery disease (CAD). In the early 1990s coronary stents were introduced to restore blood flow to the heart muscle in patients with CAD. A stent is a tubular scaffold which can be inserted into a diseased artery to relieve the narrowing caused by a stenosis.

Restenosis is the excessive growth of new tissue in the stented segment which can re-block the artery. The success of the stenting procedure depends on the severity of the restenosis. The growth of new tissue is termed neointimal hyperplasia and has been shown to be dependant on several factors, including arterial injury [1], areas of flow induced low wall shear stress (WSS) [2], areas of flow induced high wall shear stress gradients (WSSG) [3], as well as other patient specific medical factors.

Computational fluid dynamics (CFD) has been used extensively to predict areas of low WSS and high WSSG in stented arteries [4-7]. However, the unrealistic assumption that the stented segment retains a perfectly circular cross section after stent implantation is implicit to these investigations. A recent CFD investigation [8] of a stented artery compared a model using the circular cross section assumption to a model with simplified arterial prolapse and found a 300% difference in maximum WSSG results. In practice, stents are oversized by a factor of approximately 10% to the nominal diameter of the diseased artery for maximum effectiveness [9]. This aspect of stent implantation is also frequently overlooked in CFD investigations [4-7].

This paper shows the consequence of neglecting these features in the CFD model by comparing simple, oversized and prolapse models. The three models are created for two different stent designs that were commercially available in the past.

Section 2 provides the methodology to create the three-dimensional models of the two different stent designs. The methodologies to create the simple, oversized and prolapse computational models are also presented.

Section 3 describes the methodology for the CFD simulations. Steady state simulations are performed for the left anterior descending (LAD) coronary artery implanted with either a GR-II or a PS stent. Results for simple, oversized, and oversized with prolapse models are provided in each case.

2. Generation of Computational Domains

2.1 Introduction

The computational domain is the region of interest around the stent in which the CFD will solve the governing equations of fluid mechanics to predict the fluid flow.

2.2 Stent CAD Models

The computer aided design (CAD) models of the GR-II and PS stents shown in Figures 1 and 2 respectively are created using ANSYS Workbench Version 11 (Canonsburg, PA).

The rectangular cross section of each stent wire is defined by four points in a two dimensional (2D) plane. Multiple 2D planes are then generated to define the 3D shape of the stent.

The automated construction algorithms designed for creation of both stent models are written in Jscript and input to the software using the scripting application program interface. The algorithms allow for the models to be generated with a user defined diameter. The length of the GR-II stent is fixed at 20mm due to the longitudinal spine. The length of the PS stent is a variable which is dependant on the diameter.

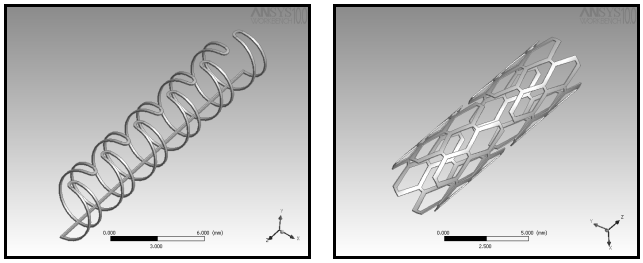

Figure 1: Three dimensional models of: (a) the GR-II coronary stent; (b) the PS coronary stent, created with ANSYS Workbench Version 11

2.3 Simple Implanted Stent Models

Idealised cylindrical arteries are constructed using ANSYS Workbench and the stent models with 3.0mm inner diameters shown in Figure 1 above are cut from the arteries to produce computational domains representing the arteries implanted with either stent as shown in Figure 2 below. The artery diameters in the GR-II model and the PS model are 3.152mm and 3.127mm respectively to coincide with the outer diameters of the stents.

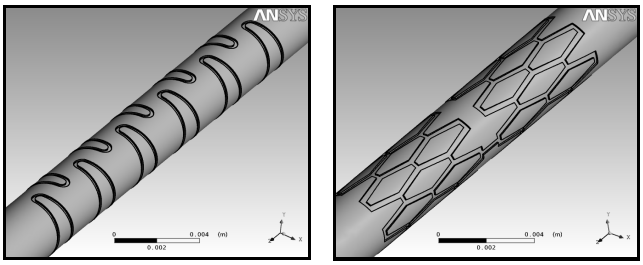

Figure 2: Simple computational models of coronary artery implanted with the 3.0mm: (a) GR-II coronary stent; (b) PS coronary stent

Additional length is added proximal and distal to the stented section to ensure the region of interest is not affected by the inlet and outlet boundary flow conditions. The additional length is provided by the formula

$$AL = 0.06 \times \mathrm{Re} \times D \approx 21mm \qquad (1)$$

where D is the artery diameter and Re is the Reynolds number given by

$$\mathrm{Re} = \frac{\rho V D}{\mu} \qquad (2)$$

where ρ is the fluid density, V the fluid average velocity and μ the fluid dynamic viscosity.

2.4 Oversized Implanted Stent Models

Stents are typically implanted with a stent-to-artery diameter ratio range of 1.1–1.2:1 to achieve maximum luminal patency and as a limit to prevent vascular damage during deployment [9].

Computational domains are created to represent the arteries implanted with stent models with 3.5mm inner diameters. The diameters of the unstented sections are the same as in the simple implanted stent models.

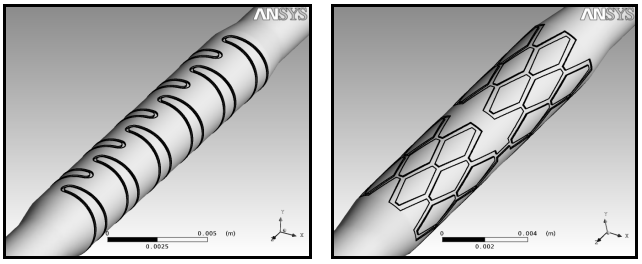

Figure 3: Oversized computational models of coronary artery implanted with the 3.5mm: (a) GR-II coronary stent; (b) PS coronary stent

2.5 Oversized Implanted Stent Models with Prolapse

It is unrealistic to assume a stented segment of an artery retains an ideal cylindrical shape, finite element analysis has shown there will be tissue prolapse between the stent wires [10]. This section describes a novel and efficient methodology to numerically predict tissue prolapse in a stented segment of an artery. The versatility of this methodology is then demonstrated by its application to two highly contrasting stent designs.

The initial step is to take Young's equation [11] which uses a cosine function to define the shape of a stenosis and apply it to predict prolapse between two stent wires. The prolapse equation is then given by

$$\frac{R}{R_o} = 1 - \frac{\delta}{2R_o}\left\{1 + \cos\frac{2\pi}{L}\left(z - \frac{L}{2}\right)\right\} \qquad (3)$$

where L is the distance between two stent wires, δ is the maximum protrusion height of the prolapse, R_o is the inner radius of the healthy artery and z and R are co-ordinate variables as shown in Figure 4 below.

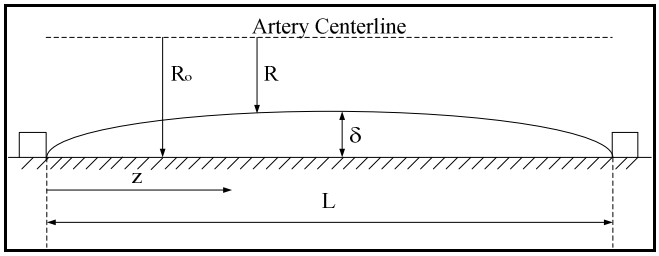

Figure 4: Protrusion of arterial prolapse between two stent wires from the artery wall as described by the prolapse equation

Equation (3) above is modified to predict tissue prolapse in a three-dimensional stented artery by setting the prolapse maximum protrusion height as a function of the intra-wire spacing

$$\delta = CL \quad (4)$$

where C is the coefficient of prolapse derived from data provided by Prendergast et al. [10] and shown in Figure 5.

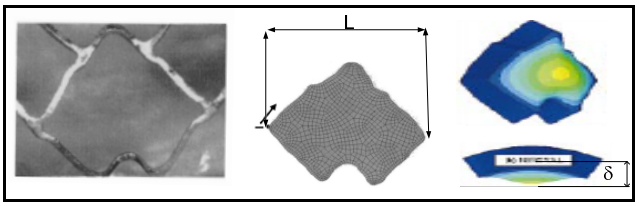

Figure 5: Finite Element Analysis of the NIROYAL stent (Boston Scientific) conducted by Prendergast et al. and providing maximum protrusion height (δ) and supported length of tissue (L)

To predict the prolapse of a given stent, the scaffolding properties of the geometry must first be classified as circumferentially or axially dominant. The GR-II stent is axially dominant as the shortest distance between two stent wires is in the axial direction. Conversely the PS stent is circumferentially dominant as the shortest distance between its stent wires is in the circumferential direction. The modified prolapse equation is applied to the dominant scaffolding direction for each stent model.

A further modification of the equation must be applied to account for the secondary scaffolding direction of each stent. In this case it is assumed that the third supporting wire begins to influence the prolapse at half the distance L between the wires in the primary direction. The modified equation is written

$$\frac{R}{R_o} = 1 - \frac{X\delta}{2R_o}\left\{1 + \cos\frac{2\pi}{L}\left(z - \frac{L}{2}\right)\right\} \quad (5)$$

where X decreases linearly from one to zero in the secondary direction, providing zero prolapse at the third supporting stent wire as shown in Figure 6.

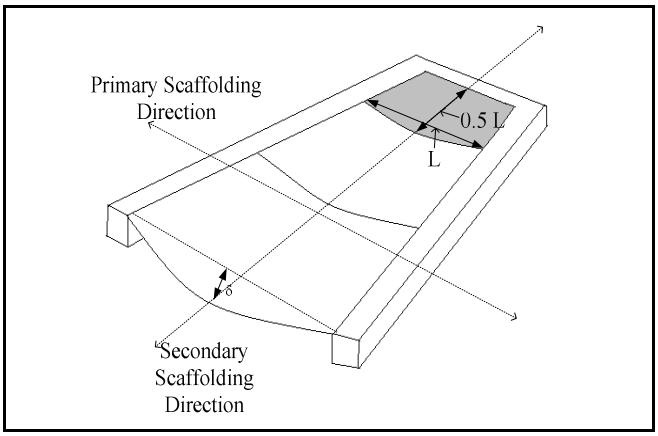

Figure 6: Illustration of the area (shaded) influenced by the stent wire in the secondary scaffolding direction with the PS stent

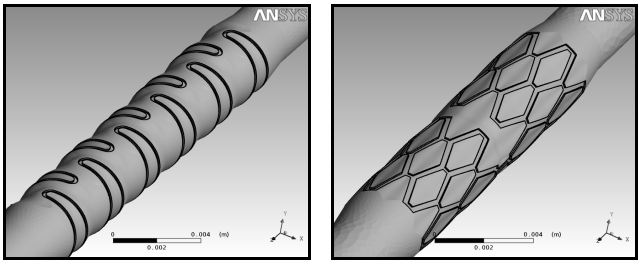

Figure 7: Prolapse models of coronary artery implanted with the: (a) GR-II Coronary Stent; (b) PS coronary stent

3. Computational Fluid Dynamics

3.1 Introduction

CFD is a process whereby real-life fluid flows are simulated using numerical methods to solve the governing equations of fluid dynamics. CFD is a relatively new branch of fluid dynamics commonly regarded as the "third" technique for solution of fluid flow problems, complementing, but not replacing the well-established approaches of theory and experiment. CFD finds it niche in modelling fluid flows that are difficult or impossible to model using theory and are complex, time consuming or expensive to measure experimentally.

3.2 Discretisation of the Computational Domain

Analytical solutions to the governing equations of fluid mechanics exist for only the simplest of flows under ideal conditions. To obtain solutions for real flows a numerical approach must be adopted whereby the equations are replaced by algebraic approximations which may be solved using a numerical method. To achieve this, the computational domain must be divided into a set of much smaller non-overlapping sub-domains called elements which constitute the mesh. Part of the mesh from the simple computational model of a coronary artery implanted with the PS coronary stent is shown in Figure 8 below.

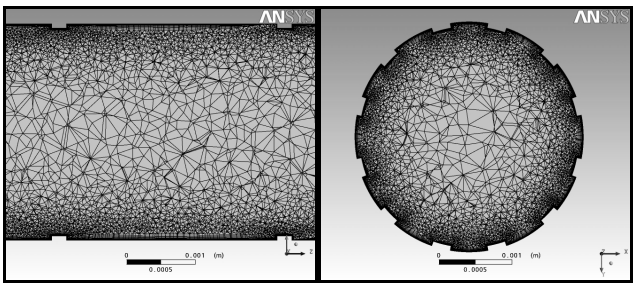

Figure 8: Cross sections of the mesh from the simple model of the artery implanted with the PS stent which has been divided into 6,161,723 elements

3.3 Governing Equations of Fluid Mechanics

All simulations involve steady laminar flow which requires the CFD code to solve the conservation of mass and momentum equations, the general form of the governing equations of fluid mechanics are listed as Equations (6) and (7) respectively:

$$\frac{\partial \rho}{\partial t} + \nabla.\left(\rho \vec{V}\right) = 0 \quad (6)$$

$$\frac{\partial \rho \vec{V}}{\partial t} + \nabla.\left(\rho \vec{V} \otimes \vec{V}\right) = -\vec{\nabla} p + \vec{\nabla}.(\tau) + \rho \vec{g} + \vec{F} \quad (7)$$

where ρ is the fluid density, p is the static pressure, $\vec{V}$ is the three dimensional velocity vector, $\vec{F}$ represents external body forces such as gravity, μ is the fluid dynamic viscosity and τ is the shear stress tensor given by Equation 8:

$$\tau = \mu\left(\nabla \vec{V} + \nabla \vec{V}^{T}\right) \quad (8)$$

At low shear rates blood exhibits the non-Newtonian behaviour of variable viscosity which is dependant on the shear rate. The non-Newtonian nature of the flow is accommodated by using the Carreau model [12] given in Equation 9:

$$\mu = \mu_{\infty} + \left(\mu_0 - \mu_{\infty}\right)\left[1 + \left(\gamma\lambda\right)^2\right]^{\left(\frac{q-1}{2}\right)} \quad (9)$$

where γ is the rate of deformation tensor given by Equation (10) in a three-dimensional Cartesian coordinate system

$$\gamma = \left[\begin{array}{l} 2\left\{\left(\frac{\partial v_x}{\partial x}\right)^2 + \left(\frac{\partial v_y}{\partial y}\right)^2 + \left(\frac{\partial v_z}{\partial z}\right)^2\right\} \\ + \left(\frac{\partial v_x}{\partial y} + \frac{\partial v_y}{\partial x}\right)^2 + \left(\frac{\partial v_x}{\partial z} + \frac{\partial v_z}{\partial x}\right)^2 + \left(\frac{\partial v_y}{\partial z} + \frac{\partial v_z}{\partial y}\right)^2 \end{array} \right]^{\frac{1}{2}} \quad (10)$$

and the constants for the Carreau model in Equation (11) have been established from experimental data [12] and are as follows

$$\begin{array}{ll} \mu_0 = 0.056 \text{ Pa.s} & \lambda = 3.31 \text{ s} \\ \mu_{\infty} = 0.00345 \text{ Pa.s} & q = 0.375 \end{array} \quad (11)$$

The commercial software code ANSYS CFX Version 11 (Canonsburg, PA) is used to solve the governing equations of fluid mechanics for non-Newtonian blood flow in the computational domain using a vertex-centred finite volume scheme.

3.4 Boundary Conditions

Boundary conditions must be applied at all exterior boundaries of the computational domain to define the flow. The same boundary conditions are applied at the inlet, outlet and on the walls for all simulations.

3.4.1 Inlet

A fully developed axial velocity profile is applied at the inlet given by:

$$V = V_{Max}\left(1 - \frac{r^2}{R^2}\right) \quad (12)$$

where the variable r is the radial coordinate measured from the centreline and R is the wall radius. V_{Max} is the maximum centreline velocity given a value which corresponds to a blood volume flow rate of 55 ml/min to simulate resting conditions in the LAD coronary artery [13].

3.4.2 Outlet

A fixed static pressure of zero Pascals was applied at the outlet of the domain to allow the software to calculate the velocity at this plane.

3.4.3 Wall

The no-slip boundary condition given in equation (13) was applied on all surfaces representative of the artery wall and the stent wires.

$$\vec{V} = 0 \quad (13)$$

4. Results

4.1 Mesh Convergence Study

A mesh convergence study was carried out to establish the appropriate mesh density required such that any further increase in mesh density would not lead to a more accurate solution. Mesh convergence was achieved for both simulations by sequentially increasing the number of nodes until there was no appreciable difference in the axial distribution of WSS over 250 data points across one of the stent struts between the solutions.

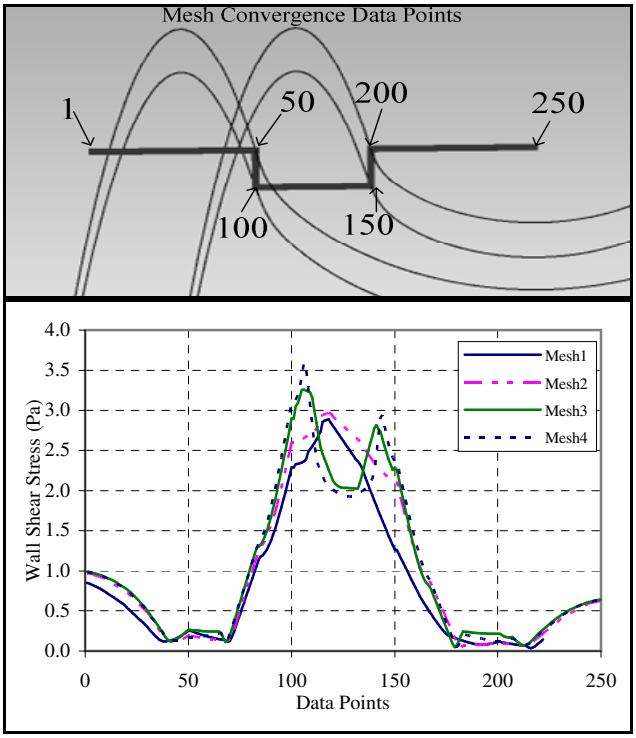

Figure 9: Axial distribution of wall shear stress over 250 data points crossing one GR-II stent strut from successively denser computational meshes

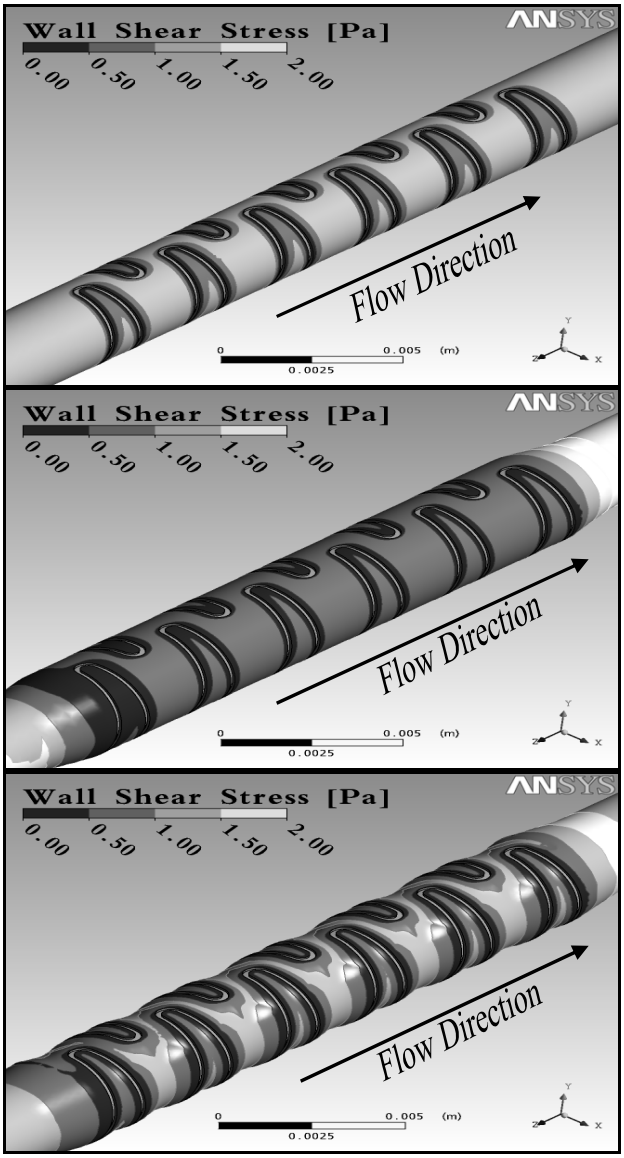

Figure 10: Contour plots of WSS showing increasing levels of detail for the GR-II: (a) simple model; (b) oversized model; (c) prolapse model

Figure 10 shows contour plots of WSS for the three models of an artery implanted with a GR-II stent. The indices for areas exposed to low WSS (<0.5 Pa) for all six models are provided in Table 1.

Area WSS < 0.5 Pa, (mm^2)	Palmaz Schatz	Gianturco-Roubin II
Simple Model	11.51	29.78
Oversized Model	39.02	68.78
Prolapse Model	39.74	65.01

Table 1: Total stented arterial area exposed to wall shear stress below 0.5 Pascals for the: (a) simple; (b) oversized; (c) prolapse models of the GR-II and PS coronary stents

The oversized models for both stents showed a much greater area subjected to low WSS than the simple models. The low WSS occurs primarily around the stent wires in the simple models. The oversized models predict a large area of low WSS in the proximal stented region for both stents. The prolapse models predicted approximately the same amount of stent area subjected to low WSS as the oversized models for both stents. The GR-II stent had a greater amount of area exposed to low WSS for all simulations.

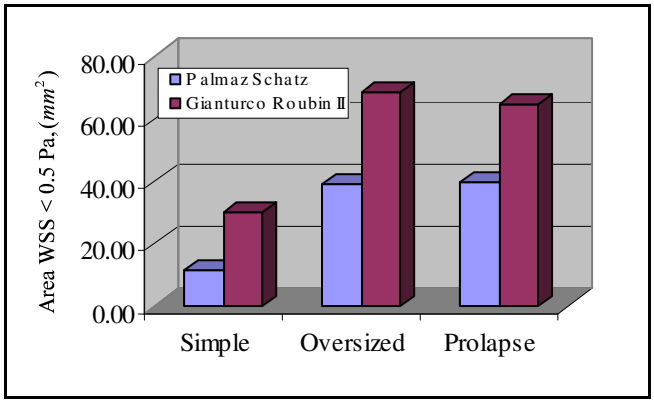

Figure 11: Graphical representation of the total stented arterial area exposed to WSS below 0.5 Pascals for the: (a) simple; (b) oversized; (c) prolapse models of the GR-II and PS coronary stents

The contour plot of WSS for the prolapse model of the PS stent is shown in Figure 12. A line of data points axially distributed along the artery wall and over the stent wires is also shown in Figure 12. WSS and axial location data is retrieved from this line for the simple, oversized and prolapse models of the PS stent and presented in Figure 13.

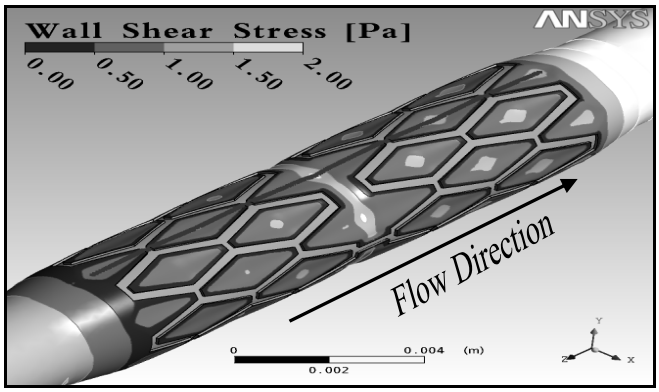

Figure 12: Contour plot of WSS for the PS prolapse model and line of axial data points used for Figure 13

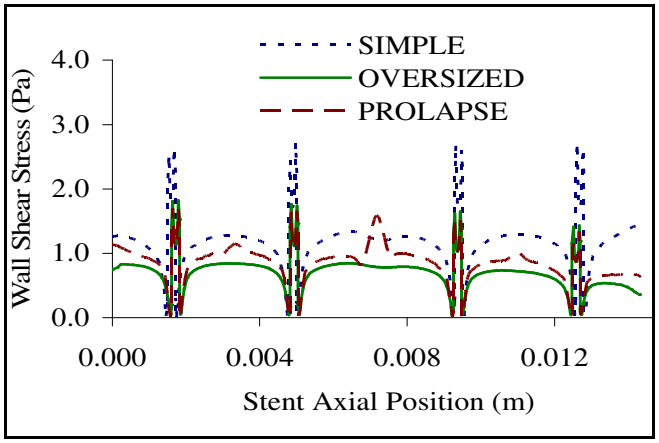

Figure 13: Axial plot demonstrating the influence of oversizing and prolapse on distributions of WSS in an artery implanted with a PS stent

The simple model has predicted much higher values for WSS than oversized and prolapse models, particularly on the stent wires in the proximal region of the stented section where the difference in WSS values is as high as 70% as shown in Figure 13. The prolapse model has predicted higher values of WSS than the oversized model in the regions between the stent wires where the arterial prolapse is greatest. This may lead to spatial WSSG that are higher than the simple and oversized models

5. Conclusion

The results clearly show a difference in WSS distributions between the simple, oversized and oversized with prolapse models for both stents. In light of the fact that WSS distributions play a crucial role in dictating the arteries response to the stenting procedure, future CFD models must include the important factors presented in this paper to predict accurate and realistic results.

All simulations predicted a greater area subjected to low WSS (< 0.5 Pascals) with the GR-II stent. In a medical trial conducted to compare the in vivo performance of these two stents, the GR-II stent had a restenosis rate of 47.3% compared to the PS restenosis rate of 20.6% after six months [9]. The results presented in this paper implicate the haemodynamic factor of low WSS as a possible cause for the GR-II stents poor clinical performance.

This work has demonstrated the ability of applied computer science to provide the biomedical community with insights into complex haemodynamics that can be used to assist in the development of optimal stent designs for the future.

Acknowledgements

This study has been funded by the Department of Mechanical Engineering, DIT, and also by the Embark Initiative managed by the IRCSET as part of the Irish National Development Plan.

References

[1] R. Schwartz, & D. R. Holmes, Pigs, Dogs, Baboons, and Man; Lessons in Stenting from Animal Studies, *Journal of Interventional Cardiology, 7*(1), 1994, 355–368.

[2] J. F. LaDisa, L. E. Olson, R. C. Molthen, D. A. Hettrick, P. F. Pratt, M. D. Hardel, J. R. Kersten, D. C. Warltier, & P. S. Pagel, Alterations in Wall Shear Stress Predict Sites of Neointimal Hyperplasia After Stent Implantation in Rabbit Iliac Arteries, *American Journal of Physiology, 288*, 2005, H2465-H2475.

[3] N. DePaola, M. Gimbrone, P. F. Davies, & C. F. Dewey, Vascular Endothelium Responds to Fluid Shear Stress Gradients, *Arteriosclerosis and Thrombosis, 12*(1), 1992, 1254-1257.

[4] D. Rajamohan, R. K. Banerjee, L. H. Back, A. A. Ibrahim, & M. A. Jog, Developing Pulsatile Flow in a Deployed Coronary Stent, *Journal of Biomechanical Engineering, 128*(3), 2006, 347-359.

[5] J. L. Berry, A. Santamarina, J. E. Moore, S. Roychowdhury, & W. D. Routh, Experimental and Computational Flow Evaluation of Coronary Stents, *Annals of Biomedical Engineering*, *28*(1), 2000, 386-398.

[6] Y. He, N. Duraiswamy, A. O. Frank, J. E. Moore, Blood Flow in Stented Arteries: A Parametric Comparison of Strut Design Patterns in Three Dimensions, *Journal of Biomechanical Engineering*, *127*(1), 2005, 637-647

[7] J. F. LaDisa, G. Ismail, L. E. Olson, D. A. Hettrick, J. R. Kersten, D. C. Warltier, & P. S. Pagel, Three-Dimensional Computational Fluid Dynamics Modeling of Alterations in Coronary Wall Shear Stress Produced by Stent Implantation, *Annals of Biomedical Engineering, 31*(8), 2003, 972-980.

[8] J. F. LaDisa, L. E. Olson, G. Ismail, D. A. Hettrick, J. R. Kersten, D. C. Warltier, & P. S. Pagel, Circumferential Vascular Deformation After Stent Implantation Alters Wall Shear Stress Evaluated With Time Dependent 3D Computational Fluid Dynamics Models, *Journal of Applied Physiology*, *98*, 2005, 947-957.

[9] A. J. Lansky, G. S. Roubin, C. B. O'Shaughnessy, P. B. Moore, & L. S. Dean, Randomized Comparison of the GR-II Stent and Palmaz-Schatz Stent for Elective Treatment of Coronary Stenoses, *Circulation, 102*(1), 2000, 1364-1368.

[10] P. J. Prendergast, C. Lally, S. Daly, A. J. Reid, T. C. Lee, D. Quinn, & F. Dolan, Analysis of Prolapse in Cardiovascular Stents: A Constitutive Equation for Vascular Tissue and Finite Element Modelling, *Journal Of Biomechanical Engineering, 125*, 2003, 692-699.

[11] D. F. Young, Effect of a Time Dependant Stenosis on Flow Through a Tube, *Journal of Engineering for Industry*, *90*(1), 1968, 248-254.

[12] H. Jung, J. W. Choi, & C. G. Park, Asymmetric Flows of Non-Newtonian Fluids in a Symmetric Stenosed Artery, *Korea-Australia Rheology Journal*, *16*(1), 2004, 101-108.

[13] S. D. Ramaswamy, S. C. Vigmostad, A. Wahle, Y. G. Lai, M. E. Olszewski, K. C. Braddy, T. M. H. Brennan, J. D. Rosen, M. Sonka, & K. B. Chandran, Comparison of Left Anterior Descending Coronary Hemodynamics Before and After Angioplasty, *Journal of Biomechanical Engineering, 128*(1), 2006, 40-48.